ChemComm

COMMUNICATION

View Article Online
View Journal | View Issue

Cite this: *Chem. Commun.*, 2022, 58, 5773

Received 25th January 2022,
Accepted 10th April 2022

DOI: 10.1039/d2cc00497f

rsc.li/chemcomm

Schiff base capped gold nanoparticles for transition metal cation sensing in organic media†

Miroslava Čonková,‡[ab] Verónica Montes-García,‡[c] Marcin Konopka,[ab] Artur Ciesielski,*[bc] Paolo Samori*[c] and Artur R. Stefankiewicz*[ab]

We report a fast and ultrasensitive colorimetric method for the detection of transition metal ions (Fe^{3+}, Cu^{2+}, Ni^{2+}) in a mixture of toluene–acetonitrile using Schiff base functionalized gold nanoparticles. We achieved limits of detection for the three metal ions at least two orders of magnitude lower than the EU recommended limits. Finally, our methodology was assessed for the determination of nickel in the organic waste of a relevant industrial reaction.

The fine chemical, petroleum, and pharmaceutical industries have been identified as major producers of chemical waste because the vast majority of technological processes are still carried out in organic solvents with the use of metal-based catalysts.[1] Organic medium hitherto remains essential not only for chemical reactions to proceed but also for the extraction and purification steps, necessary to achieve sufficient product purity. Despite the continuous development and improvement of synthetic methodologies, waste including that containing transition metal ions derived from decomposed catalysts is also often a source of contamination of the final product, including in active pharmaceutical ingredients (APIs).[2] Although some of the transition metal ions employed in catalytically relevant processes (*e.g.*, Cu^{2+}, Ni^{2+}, and Fe^{3+}) bear several important biological roles,[3–5] their excessive content in the human body can lead to serious health problems.[6] EU recommended limits in APIs are 20 ppm[7] and 300 ppm[7] for Ni^{2+} and Cu^{2+}, respectively. No specific limit has yet been established so far for Fe^{3+}, although overexposure to this metal can lead to iron poisoning,[8] including heart diseases[9] and cancer.[10] Analytical methods commonly exploited for trace metal ion determination, despite the high capital cost, are ion-coupled-plasma spectroscopy (ICP-MS)[11,12] and atomic absorption spectrometry (AAS).[12] However, the direct determination of trace elements in non-aqueous mixtures by these techniques remains problematic due to time-consuming and highly invasive sample pre-treatment (*e.g.*, mineralization, high temperature/pressure) often leading to variation in metal content.[12] Within this context, the development of simple and effective methods to detect transition metal ions in organic media is highly sought after.

Low-dimensional nanostructures possess the highest surface-to-volume ratios and unique optoelectronic properties, which are highly susceptible to their interaction with the environment. The latter can be tuned *via* the chemical functionalization of their surface with receptors of the analyte of choice, enabling the development of chemical sensors with electrical or optical readouts featuring key performance indicators beyond the state-of-the-art.[13] Among low-dimensional nanostructures, noble metal nanoparticles (NPs) represent versatile platforms for the fabrication of (bio)-chemical sensors due to their high chemical stability, surface-to-volume ratio, and distinctive optoelectronic properties. The extraordinary plasmonic phenomenon has given rise to a rapidly developing field of optical nanosensors,[14] where the exposure to target analytes can induce a localized surface plasmon resonance (LSPR) shift of the metallic NPs (in solution or deposited into a solid platform) and may be accompanied by a visual colour change. In particular, colorimetric sensing, where a specific analyte can trigger a significant visual colour change, is very attractive due to its simplicity, cost-effectiveness, and unprecedented selectivity among the traditional detection methodologies.[15]

On the other hand, Schiff bases derived from 2-hydroxybenzaldehydes and appropriate amine or hydrazide create a very effective chelating system for binding to metal cations.[16,17] They have also been employed for colorimetric ion sensing, reaching in some cases limits of detection in the micromolar range.[18–21] However, their synergetic combination with metal NPs for colorimetric cation sensing has been barely exploited. For instance, gold nanoparticles (AuNPs) functionalized with

[a] *Faculty of Chemistry, Adam Mickiewicz University, Uniwersytetu Poznańskiego 8, 61-614 Poznań, Poland. E-mail: ars@amu.edu.pl*
[b] *Center for Advanced Technology, Adam Mickiewicz University, Uniwersytetu Poznańskiego 10, 61-614 Poznań, Poland*
[c] *Université de Strasbourg, CNRS, ISIS, 8 allée Gaspard Monge, 67000 Strasbourg, France*

† Electronic supplementary information (ESI) available. See DOI: https://doi.org/10.1039/d2cc00497f

‡ These authors contributed equally to this work.

Schiff bases can effectively detect Cu^{2+}, Al^{3+}, or Fe^{3+}, exhibiting sensitivities in the micromolar range.[22–24] Yet most examples combining AuNPs and Schiff bases were investigated in aqueous solutions, despite the high stability of AuNPs capped by Schiff base ligands in organic media.[25,26] Examples of sensors combining AuNPs with Schiff base ligands capable of efficiently sensing selected metal ions in organic solvents remain very few.[24,27]

To fill this gap, we report here a new type of colorimetric sensor based on Schiff-base decorated AuNPs for the detection of industrially relevant transition metal cations (Cu^{2+}, Ni^{2+}, and Fe^{3+}) in organic solvents. The employed chelating system (**L1**) was designed to act both as a stabilizing agent of AuNPs and as a supramolecular receptor for the analyte of interest.

Ligand **L1** was designed to combine a moiety that is capable of chemisorbing on gold surfaces and a versatile coordination pocket that can efficiently bind metal cations. Thus, an α-lipoic acid moiety was chosen as the anchoring site, through the formation of an Au–S linkage,[28–31] while the mono(salicylaldehyde)-iminoacetyl-hydrazone ligand providing the N,O,O binding pocket[16,32–34] was employed for coordinating metal cations, as confirmed in the control experiment with ligand **L2** (see ESI†). Ligand **L1** was synthesized from α-lipoic acid *via* a three-step protocol in a high 75% overall yield without column chromatography (see Scheme S1, ESI†). The final ligand **L1** was obtained as a mixture of two geometrical isomers (in Z:E = 2 : 1 ratio calculated from integrals of H-9$_{cis}$, H-9$_{trans}$ and H-11$_{cis}$, H-11$_{trans}$). Detailed synthetic procedures and characterization can be found in the ESI,† Fig. S1–S8.

The synthesis of monodispersed AuNPs in toluene was performed by following a previously reported protocol, where oleylamine was used as a surfactant.[35] The resulting oleylamine capped gold nanoparticles (**OL**@AuNPs) featured a plasmon band at 526 nm, ascribed to the dipole resonance of individual AuNPs (Fig. 1b). The interactions between the gold nanoparticle surface and the amine group of oleylamine are weaker than dative Au–S bonds, and hence this favours the ligand exchange reaction between oleylamine and ligand **L1**. The ligand exchange reaction should be achieved by adding approximately 890 **L1** molecules per nanoparticle (calculated from the size of the metal core, for details see ESI†). To maximize the number of **L1** molecules on the AuNPs surface, and hence have the maximum number of receptors, we performed the ligand exchange reaction with different concentrations of ligand **L1** (*i.e.*, from 7.5 to 60 μM) and we studied the stability of the AuNPs in time (see ESI,† Fig. S12). The highest concentration of ligand **L1** that lead to a *stable* system during at least 96 hours was 15 μM; higher concentrations lead to a fast and irreversible aggregation of the system (see ESI,† Fig. S12C and D).

The size and the morphology studies of both **OL**@AuNPs and **L1**@AuNPs were performed by transmission electron microscopy (TEM) and dynamic light scattering measurements (DLS). TEM images of **OL**@AuNPs revealed monodispersed spherical nanoparticles with uniform shape and core size 11.5 ± 1.2 nm (Fig. 1c), which is in good agreement with DLS measurements, revealing an average hydrodynamic diameter of 14.3 ± 4.4 nm (for details see ESI,† Fig. S13 and S14). In the case of **L1**@AuNPs, TEM images revealed that the AuNP size remains constant (core size: 10.8 ± 1.1 nm, Fig. 1d) as ligand **L1** is not expected to modify the NP size. This is in good agreement with DLS measurements, which showed an average hydrodynamic diameter of **L1**@AuNPs of 15.45 ± 4.26 nm (see ESI,† Fig. S13).

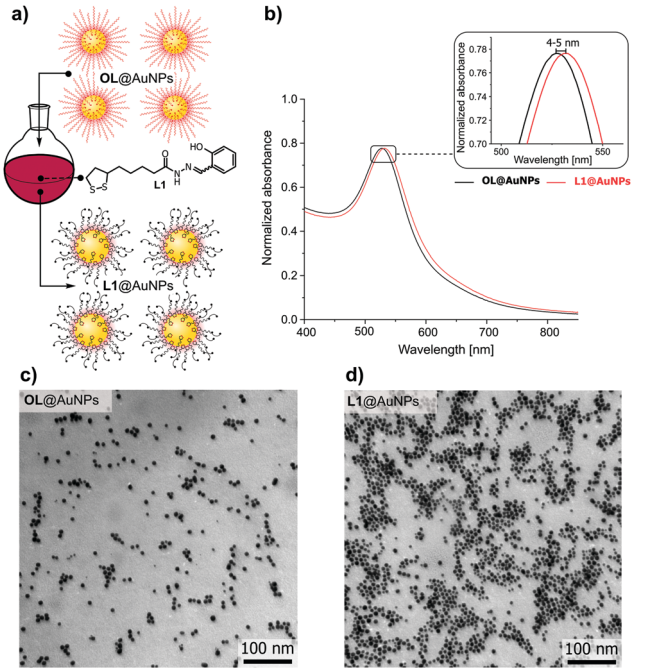

Fig. 1 (a) Schematic representation of the ligand exchange reaction; (b) UV-Vis comparison of **OL**@AuNPs and **L1**@AuNPs; (c) TEM image of **OL**@AuNPs (d) TEM image of **L1**@AuNPs.

To evaluate the sensing performance, our system was tested for the selected transition metal ions (Cu^{2+}, Ni^{2+}, and Fe^{3+}). To rule out nonspecific acetonitrile-induced aggregation we have verified the stability of **L1**@AuNPs in the presence of acetonitrile up to 23% (see ESI,† Fig. S15). To demonstrate the selective interactions between ligand **L1** and metal cations, colloidal dispersions of **OL**@AuNPs were exposed to selected metal cations and no aggregation was observed (see Fig. S16a, S17a, and S18a in ESI†). These experiments also exclude any non-specific interaction with AuNPs. To eliminate the counter ion influence, all experiments were performed by using NO_3^{2-} salts. After 10 minutes of analyte addition (for a detailed description see ESI†), a visible colour change from red to purple was observed indicating the aggregation of **L1**@AuNPs (See Fig. 2). The response time observed for our system is better or comparable with other known colorimetric sensors (see ESI,† Table S4).[36–40] The aggregation of **L1**@AuNPs is triggered by the coordination reaction between the *N*-acylhydrazone moiety and the metal cation, giving rise to octahedral complexes (Fig. 2). Solely based on naked-eye observation, the colour change from red to purple can be observed in the 5–7.5 μM concentration range (Fig. S19 in ESI†). To be easily comparable to the EU recommended limits, we converted the concentration in which colour change was noted into ppb. More specifically, for Cu^{2+}

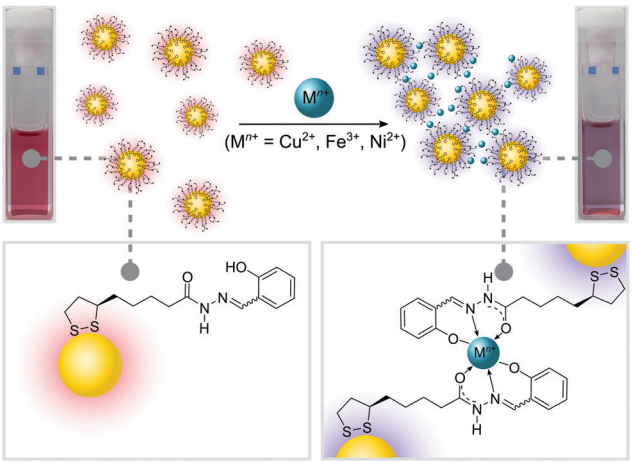

Fig. 2 Schematic representation of coordination triggered aggregation.

cations, the visible colour change took place after the addition of 5 μM, which corresponds to 366 ppb. For Fe^{3+} cations it was 7.5 μM (458 ppb) and 5 μM of Ni^{2+} cations, which corresponds to 204 ppb (see ESI,† Fig. S19). As compared to the allowed limits of transition metal ions in APIs and an excipient,[7] our sensor exhibited a sensitivity 2 and 3 orders higher.

The sensing performance of the **L1**@AuNPs was quantitatively assessed *via* UV-Vis spectroscopy. The UV-vis absorbance spectrum of **L1**@AuNPs upon each metal ion addition at different concentrations showed a red shift of the LSPR band (Fig. 3a, b, and c, for Cu^{2+}, Fe^{3+}, and Ni^{2+} ions, respectively). The calibration curves were obtained by plotting known concentrations of Cu^{2+}, Ni^{2+} or Fe^{3} ions (1–10 μM) against the LSPR maximum (Fig. 3d and Table S1 in ESI†) and the linear response can be fitted to the formula: $LSPR_{max} = a \times [\text{metal ion}] + b$. For calculating the limit of detection (LoD) of each metal ion, the $3S_B/m$[41] equation was used, where S_B is the standard deviation of a blank sample and m is the slope of each calibration curve, also known as sensitivity (S). The colorimetric sensor in toluene–acetonitrile solutions showed extremely low LoDs, in the range 1.4–11.2 nM (see ESI,† Table S1) for the assessed metal ions.

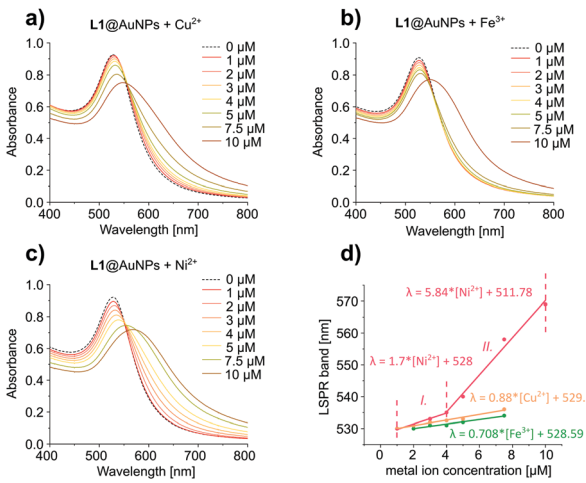

Fig. 3 (a) UV-Vis spectrum showing the LSPR band shift upon addition of Cu^{2+}, (b) Fe^{3+} and (c) Ni^{2+}; (d) linear change of LSPR maximum plotted as a function of metal ion concentration.

As can be seen in Fig. 3d, the sensor showed a similar sensitivity in the case of Cu^{2+} and Fe^{3+} cations (S = 0.88 and 0.71 μM^{-1}, respectively). However, the sensitivity towards the most catalytically valuable and the most toxic of all studied cations, *i.e.* Ni^{2+}, was much higher in both linear regions (S = 1.7 and 5.84 μM^{-1}). This high sensitivity towards Ni^{2+} can be further utilized in industrially valuable Ni-catalyzed reactions, such as the synthesis of Pictilisib[42] or PDE472.[43] Usually, Ni^{2+}, Cu^{2+} and Fe^{3+} cations are not found as a mixture in industrial processes and hence we highlight that our colorimetric sensor can be used to detect all of them individually. When compared to other known colorimetric sensors based on Schiff bases, **L1**@AuNPs displayed 2–6 orders of magnitude lower LoD than structurally similar Schiff base capped AuNP sensors, which were described for Cu^{2+}[22,27] and Al^{3+}[23] detection.

To demonstrate that our sensor can be used for the quantitative evaluation of metal content in organic waste produced during catalytic processes used in the pharmaceutical industry, we decided to reproduce the synthetic protocol reported by Novartis Pharma AG, that utilizes nickel catalyzed Kumada coupling for the synthesis of PDE472, an inhibitor of phosphodiesterase type 4D and a recognized drug target for the treatment of asthma.[43] The reaction was performed at a laboratory scale and the organic waste was analyzed by UV-vis spectroscopy with our sensor and by inductively coupled plasma mass spectrometry (ICP-MS). Right after the purification procedure, the toluene waste (50 μL) was added to the **L1**@AuNP dispersion (for more details see ESI†). The UV-vis spectrum was recorded after 10 minutes and showed a red shift of the LSPR band (4 nm, see ESI,† Fig. S22), similar to the red shift observed for low concentrations of Ni^{2+} ions ($\leq$ 4 μM, see ESI,† Fig. S17d). On the basis of this UV-Vis experiment and the calibration curve obtained upon the addition of a known concentration of Ni^{2+} ions (Fig. S17d, ESI†), the Ni^{2+} content in the real sample was evaluated as 3.5 μM. The exact nickel content was determined by ICP-MS. The obtained value of 3.49 μM is in full agreement with our UV-vis results. It is worth highlighting that for ICP-MS measurements the organic waste had to be evaporated, dried and mineralized prior to measurement, which in total took several hours. On the other hand, for our sensing experiment, the organic waste was directly examined by UV-vis spectroscopy without any pre-treatment, which reduced the total analysis time to a few minutes.

We have devised a highly sensitive chemical sensor of divalent and trivalent metal ions based on Schiff base capped AuNPs *via* colorimetric detection. These low-dimensional sensitive elements were characterized by UV-vis spectroscopy, DLS, and TEM. The colorimetric response relies on the complexation of the metal ions with the Schiff base ligand, forming ML_2-type complexes with first-row transition metal ions (Ni^{2+}, Cu^{2+}, Fe^{3+}) in toluene–acetonitrile solution, which triggers the AuNP aggregation process. The metal coordination occurred in less than 10 minutes, which makes this sensor suitable for on-the-spot

qualitative sensing. The sensitivity performance was excellent for all studied ions, and the colorimetric response visible solely by the naked eye (no instrumentation necessary) was as low as 204 ppb for Ni^{2+} ions, which is two orders of magnitude lower than the EU recommended limits. The estimated LoD for all studied metal ions was in the nanomolar range and the highest sensitivity was observed for the toxic and catalytically valuable Ni^{2+} cations.

Significantly, our chemical sensor outperforms other known Schiff base capped AuNP colorimetric sensors, with a 3–6 orders of magnitude lower LoD. Moreover, we demonstrated the applicability of our sensor for the evaluation of the Ni^{2+} content in organic waste generated during the synthesis of PDE472, a recognized drug target for the treatment of asthma. The modular strategy applied can tune the sensor on-demand and it can be refined to become suitable for the selective detection of transition metal ions for pharmaceutical and technological applications in organic solvents.

The activity in Poznań was funded by the National Science Centre of Poland grant: SONATA BIS 2018/30/E/ST5/00032 (A.R.S.) and co-funded by The National Centre for Research and Development grant: POWR.03.02.00-00-I032/16 (M.C.). The activity in Strasbourg was financially supported by European Commission through the ERC project SUPRA2DMAT (GA-833707), the AMI project funded by the ERA-NET EuroNanoMed III program, the European Union and the Agence Nationale de la Recherche (ANR) GA-ANR-17-ENM3-0001-01, the Labex project CSC (ANR-10LABX-0026 CSC) within the Investissement d'Avenir program ANR-10-IDEX-0002-02, the International Center for Frontier Research in Chemistry (icFRC) and the Institut Universitaire de France (IUF). We thank Prof. Danuta Barałkiewicz and Dr Adam Sajnóg for ICP-MS measurements.

Conflicts of interest

There are no conflicts to declare.

Notes and references

1 S. Abou-Shehada, J. H. Clark, G. Paggiola and J. Sherwood, *Chem. Eng. Process.*, 2016, **99**, 88–96.
2 European Medicine Agency, *Guideline on the Specification Limits for Residues of Metal Catalysts*, London, 2007.
3 R. Crichton, *Inorganic Biochemistry of Iron Metabolism: From Molecular Mechanisms to Clinical Consequences*, John Wiley & Sons, Ltd, 2001.
4 A. Sass-Kortsak, *Adv. Clin. Chem.*, 1966, **8**, 1–67.
5 F. Sunderman, *Ann. Clin. Lab. Sci.*, 1977, **7**, 377–398.
6 R. R. Crichton, in *Metal Chelation in Medicine*, ed. R. J. W. Robert R Crichton, Robert C Hider, 2016, ch. 1, pp. 1–23.
7 European Medicine Agency, ICH guideline Q3D (R1) on elemental impurities, 2019.
8 C. G. Fraga, *Mol. Aspects Med.*, 2005, **26**, 235–244.
9 M. L. Rasmussen, A. R. Folsom, D. J. Catellier, M. Y. Tsai, U. Garg and J. H. Eckfeldt, *Atherosclerosis*, 2001, **154**, 739–746.
10 L. E. Beckman, G. F. Van Landeghem, C. Sikstrom, A. Wahlin, B. Markevarn, G. Hallmans, P. Lenner, L. Athlin, R. Stenling and L. Beckman, *Carcinogenesis*, 1999, **20**, 1231–1233.
11 N. Lewen, S. Mathew, M. Schenkenberger and T. Raglione, *J. Pharm. Biomed. Anal.*, 2004, **35**, 739–752.
12 E. Bulska and A. Ruszczynska, *Phys. Sci. Rev.*, 2017, **2**, 1–14.
13 R. Furlan de Oliveira, V. Montes-Garcia, A. Ciesielski and P. Samori, *Mater. Horiz.*, 2021, **8**, 2685–2708.
14 C. Pezzato, S. Maiti, J. L. Chen, A. Cazzolaro, C. Gobbo and L. J. Prins, *Chem. Commun.*, 2015, **51**, 9922–9931.
15 V. Montes-Garcia, M. A. Squillaci, M. Diez-Castellnou, Q. K. Ong, F. Stellacci and P. Samori, *Chem. Soc. Rev.*, 2021, **50**, 1269–1304.
16 G. Markiewicz, A. Walczak, F. Perlitius, M. Piasecka, J. Harrowfield and A. R. Stefankiewicz, *Dalton Trans.*, 2018, **47**, 14254–14262.
17 A. R. Stefankiewicz, J. Harrowfield, A. M. Madalan and J. M. Lehn, *CrystEngComm*, 2013, **15**, 9128–9134.
18 B. Kaur, N. Kaur and S. Kumar, *Coord. Chem. Rev.*, 2018, **358**, 13–69.
19 V. K. Gupta, A. K. Singh, M. R. Ganjali, P. Norouzi, F. Faridbod and N. Mergu, *Sens. Actuators, B*, 2013, **182**, 642–651.
20 H. Sun, Y. Jiang, J. Nie, J.-H. Wei, B. X. Miao, Y. Zhao, L.-F. Zhang and Z.-H. Ni, *Mater. Chem. Front.*, 2021, **5**, 347–354.
21 Z. Liao, Y. Liu, S.-F. Han, D. Wang, J.-Q. Zheng, X.-J. Zheng and L.-P. Jin, *Sens. Actuators, B*, 2017, **244**, 914–921.
22 Y. Wang, X. Li, Y. Zhou and C. Liu, *Int. J. Chem.*, 2012, **4**, 90–95.
23 P. Huang, J. Li, X. Liu and F. Wu, *Microchim. Acta*, 2015, **183**, 863–869.
24 A. A. Jimoh, A. Helal, M. N. Shaikh, M. A. Aziz, Z. H. Yamani, A. Al-Ahmed and J. P. Kim, *J. Nanomater.*, 2015, **2015**, 1–7.
25 W. Edwards, N. Marro, G. Turner and E. R. Kay, *Chem. Sci.*, 2018, **9**, 125–133.
26 J. M. McMahon and S. R. Emory, *Langmuir*, 2007, **23**, 1414–1418.
27 E. Oliveira, J. D. Nunes-Miranda and H. M. Santos, *Inorg. Chim. Acta*, 2012, **380**, 22–30.
28 A. C. Savage and Z. Pikramenou, *Chem. Commun.*, 2011, **47**, 6431–6433.
29 P. D. Beer, D. P. Cormode and J. J. Davis, *Chem. Commun.*, 2004, 414–415, DOI: **10.1039/b313658b**.
30 Z. Krpetic, L. Guerrini, I. A. Larmour, J. Reglinski, K. Faulds and D. Graham, *Small*, 2012, **8**, 707–714.
31 J. M. Abad, S. F. Mertens, M. Pita, V. M. Fernandez and D. J. Schiffrin, *J. Am. Chem. Soc.*, 2005, **127**, 5689–5694.
32 D.-H. Wang, Y. Zhang, R. Sun and D.-Z. Zhao, *RSC Adv.*, 2016, **6**, 4640–4646.
33 Y. Gou, Y. Zhang, J. Qi, Z. Zhou, F. Yang and H. Liang, *J. Inorg. Biochem.*, 2015, **144**, 47–55.
34 J.-X. Yu, V. D. Kodibagkar, L. Liu, Z. Zhang, L. Liu, J. Magnusson and Y. Liu, *Chem. Sci.*, 2013, **4**, 2132.
35 X. Huang, A. J. Shumski, X. Zhang and C. W. Li, *J. Am. Chem. Soc.*, 2018, **140**, 8918–8923.
36 K. Singh, V. Kumar, B. Kukkar, K. H. Kim and T. R. Sharma, *Int. J. Environ. Sci. Technol.*, 2021, DOI: **10.1007/s13762-021-03331-0**.
37 J. Das and P. Sarkar, *Environ. Sci.: Water Res. Technol.*, 2016, **2**, 693–704.
38 T. Kiatkumjorn, P. Rattanarat, W. Siangproh, O. Chailapakul and N. Praphairaksit, *Talanta*, 2014, **128**, 215–220.
39 T.-B. Wei, P. Zhang, B.-B. Shi, P. Chen, Q. Lin, J. Liu and Y.-M. Zhang, *Dyes Pigm.*, 2013, **97**, 297–302.
40 A. K. Yetisen, Y. Montelongo, M. M. Qasim, H. Butt, T. D. Wilkinson, M. J. Monteiro and S. H. Yun, *Anal. Chem.*, 2015, **87**, 5101–5108.
41 European Medicine Agency, ICH Topic Q 2 (R1) Validation of Analytical Procedures: Text and Methodology, 1995.
42 Q. Tian, Z. Cheng, H. M. Yajima, S. J. Savage, K. L. Green, T. Humphries, M. E. Reynolds, S. Babu, F. Gosselin, D. Askin, I. Kurimoto, N. Hirata, M. Iwasaki, Y. Shimasaki and T. Miki, *Org. Process Res. Dev.*, 2013, **17**, 97–107.
43 P. W. Manley, M. Acemoglu, W. Marterer and W. Pachinger, *Org. Process Res. Dev.*, 2003, **7**, 436–445.

